Evaluation of the imaging properties of holograms recorded in materials of limited spatial resolution

István Bányász, MEMBER SPIE
Hungarian Academy of Sciences
Institute of Isotopes
P.O. Box 77
Budapest H-1525, Hungary

Abstract. A new method for the evaluation of the effects of the finite spatial resolution of the recording material on the reconstructed holographic image is presented. The method is based on substitution of the amplitude modulation transfer function (the square root of the modulation transfer function) of the recording material into the double Fresnel-Kirchhoff integral describing the complex amplitude of the reconstructed image. Numerical calculations have been carried out for holograms recorded in silver halide and thermoplastic-photoconductor materials. The contrast of the reconstructed image as a function of various recording parameters, such as the resolution limit and slope (in case of silver halides), and the center and width (in case of thermoplastics) of the amplitude modulation transfer function of the recording material, the object position and the reference beam angle has been computed. Thin holograms of microline objects have been studied in several recording geometries, including one with a tilted object plane.

Subject terms: holography theory; image characteristics; holographic recording materials.

Optical Engineering 32(10), 2539-2547 (October 1993).

1 Historical Review

The spatial resolution of the recording material is a crucial factor determining the quality of the holographic image. It is obvious that the quality of the actual recording material can considerably affect the quality of the reconstructed image especially when the hologram is of high numeric aperture and nearly diffraction limited resolution and high fidelity are required. The principal characteristic of the recording material in holography is the modulation transfer function (MTF) describing the finite spatial resolving power of the material. There is a natural demand on the part of the practical holographers to predict the quality of the reconstructed holographic image as precisely as possible before the hologram is recorded. It may be especially important when computer-generated optical elements are being either directly fabricated or copied into conventional recording materials.

Although a great number of valuable papers have been published on the theory of holography and particularly on the recording materials since the 1960s, the results of the majority of them are not applicable in solving the real problems of practical holography. A few of the most important

ones dealing with the effects of film MTF are enumerated in the following.

The first attempts to describe the effect of the MTF of the recording material were based on assuming certain fictitious masks or pupils placed in the object beam at the recording step. It was Van Ligten who first suggested the use of such a hypothetical mask.[1] Similar methods have been followed by Lukosz,[2] Urbach and Meier,[3] and Jannson.[4] Lukosz[2] suggested making the amplitude transmittance of the fictitious mask equal to the MTF, but he did not give an explicit form of the transmittance. Jannson,[4] similarly to the greatest number of experimentalists, assumed a rectangular MTF. Later it is demonstrated that this usual approximation gives false results; the image quality is usually considerably underestimated. Kozma and Zelenka[5] derived some general expressions for the reconstructed holographic image in the case of rectangular and Gaussian film MTF. Similarly to other authors (Diamond[6]), they assumed that the impulse response of the holographic film is the Fourier transform of its MTF.

Unfortunately, none of these papers concluded with results that could have been readily applied in practical holography.

Relatively few papers can be found on the possible theoretical functions describing the film MTF of the holographic recording materials. Biedermann[7] made use of Friesem's model of the silver halide photomaterials. Falconer[8] sug-

gested a film MTF consisting of two additive terms: a Gaussian function (the Fourier transform of the Gaussian point spread function of the recording material) and a function of the form of the Maxwell-Boltzmann distribution describing the so-called adjacency effects (caused by the global nonlinearity of the film).

Measured MTF curves of standard silver halide materials routinely used in holography can be found in the papers of Biedermann[7] and Friesem et al.[9] and in monographs on holography.[10–12]

Thermoplastic holographic recording materials have been extensively studied both theoretically and experimentally since the 1960s. It was Glenn[13] who first reported the use of thermoplastic materials for high-density recording of electrical signals by electron beam writing. The first holographic recording in an organic photoconductor overcoated with an insulating thermoplastic was made by Urbach and Meier.[14] Later, a number of different versions of these devices were developed.[15,16]

A number of papers appeared on the various experimental characteristics (e.g., spectral sensitivity, MTF) of the thermoplastics.[17–22] Because thermoplastic holographic recording devices are much more complicated than silver halide or dichromated gelatine materials, there is a vast diversity in the reported characteristics. The results of different authors usually are incomparable.

Although it is not easy to establish general laws describing the properties of thermoplastic recording materials, several theoretical papers on their physical properties can be found in the literature.[23–26] In some of these works, theoretical relationships between some physical properties and the spatial frequency of the periodic surface relief pattern of the thermoplastic have been established. However, no analytical function for the MTF of these recording materials has been derived.

Holography with thermoplastics has been thoroughly treated in the review of Urbach.[27] In the conclusions of his review, he points out the advantages of holograms recorded in thermoplastic overcoated photoconductor devices, namely their relatively high diffraction efficiency (over 30%), the attainable high-resolution limit (up to 4000 lines/mm) and high useful bandwidth (in excess of 1000 lines/mm in some devices), the suppression of intermodulation distortions as a result of this bandpass spatial frequency response, and high sensitivity (comparable to that of the silver halide materials).

Based on the statements of the latter paragraphs, one could think that thermoplastic photoconductor devices are excellent candidates for reconfigurable holographic optical elements even when high resolution and field range are required. However, at least to my knowledge, no study concerning the ultimate capabilities in image resolution of these recording media has appeared so far.

The aim of the present work is to develop an exact method for the direct evaluation of the effects of film MTF on the reconstructed image of an arbitrary object retrieved from an arbitrary hologram. To obtain results applicable to a wide range of hologram types, the calculations were based (likewise in my method for the evaluation of hologram aberrations[28,29]) on the most general form of the scalar Fresnel-Kirchhoff integral. First the complex amplitudes of the object and reference waves are computed in the hologram plane. The effects of the film MTF are taken into account by mul-
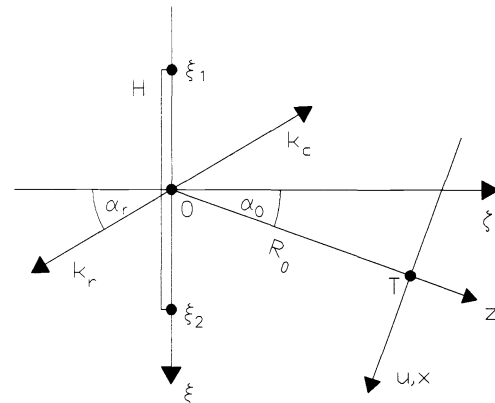

Fig. 1 General recording geometry.

tiplying the complex amplitude transmittance of the hologram by suitable analytical functions. The complex amplitude of the reconstructed real image is then obtained by multiplying the above transmittance by the complex amplitude of the reconstruction wave and evaluating the second Fresnel-Kirchhoff integral.

As a consequence of these assumptions, the following calculations apply for thin amplitude (and shallow phase relief) holograms, albeit, because of the equivalence of thin and thick holograms with respect to image quality,[30] it is hoped that they can be extended to volume holograms by making use of either the thin grating decomposition or the coupled wave theory.

2 Recording Geometries and the Object

Five different recording geometries were studied. The general recording and reconstruction geometry is shown in Fig. 1. The one-dimensional hologram (H) is located along the ξ axis. The object plane (i.e., the u axis) is inclined at an angle α_0 to the hologram plane. The object is illuminated by a plane wave perpendicular to the object plane. The separation of the hologram center (O) and the object center (T) is denoted by R_0. The angle of incidence of the plane reference wave is α_r. The hologram width is L. The edges of the hologram are ξ_1 and ξ_2. The real image of the object is reconstructed by the conjungate of the reference wave (k_c). The intensity distribution of the reconstructed real image is calculated along the u axis.

The objects were five-element Ronchi rulings consisting of individual lines of linewidths 0.5 to 4.0 μm (i.e., the grating constants were in the range of 1.0 to 8.0 μm). Evaluation of the reconstructed images of such objects gives a more realistic measure of the quality of the holograms than that of one- or two-point objects.[31] The parameters of the five recording geometries are shown in Table 1. The wavelength of the light is 632.8 nm for all the calculations presented in the paper. Note that ξ_1 was chosen different from $-\xi_2$ in geometry D to record symmetrically the far-field diffraction pattern of the object. The numerical apertures of all the five recording geometries are high.

3 Evaluation of the Reconstructed Image

3.1 Diffraction-Limited Reconstruction

As previously stated, all the subsequent calculations are based on the numerical evaluation of the Fresnel-Kirchhoff integral.

Table 1 Parameters of the recording geometries.

Geometry	R_s (mm)	L (mm)	ξ_1	α_o (deg.)	α_r (deg.)	N. A.
C	32	84	-42.0	0.0	-66.0	0.795
D	32	84	-46.0	33.0	-33.0	0.791
G	17.5	84	-42.0	0.0	-80.0	0.921
E	32	84	-42.0	0.0	-40.0	0.795
F	32	84	-42.0	20.0	-20.0	0.800

For the geometry shown in Fig. 1, the diffraction-limited complex amplitude distribution of the reconstructed real image is the following[28,29]:

$$\mathbf{V}(x,z) = \int_{\xi_1}^{\xi_2} \int_{u_1}^{u_2} \mathbf{U}(u) \frac{\cos\theta \, \cos\rho}{r_1 r_2} \exp[ik(r_1 - r_2)] \, du \, d\xi \ , \quad (1)$$

where $\mathbf{U}(u)$ is the complex amplitude transmittance of the object; θ and ρ are the inclination angles for the diffraction at the object and hologram plane, respectively; and r_1 and r_2 are the separations of the source and observation points at the first and the second diffraction. It is assumed that there is no wavelength change at reconstruction. Evaluating this formula for a special holographic geometry and taking the square of the complex absolute value of $\mathbf{V}(x)$, one obtains the diffraction-limited image of the object.

3.2 Effect of the Film MTF

In off-axis holography, the spatial frequency variations through the holographic grating are mainly determined by the angle of incidence of the reference wave and the position of the object. If the object is small compared with the width of the hologram, a sufficiently small surrounding of each hologram point can be regarded as an elementary plane wave hologram. Consequently, a well-defined grating frequency can be assigned to each hologram point:

$$\nu(\xi) = \frac{\sin\beta_0(\xi) - \sin\alpha_r}{\lambda} \ , \quad (2)$$

where ξ is the coordinate along the hologram, $\beta_0(\xi)$ is the local angle of incidence of the central object ray, α_r the (constant) angle of incidence of the reference wave, and λ is the wavelength of the light.

Knowing the local spatial frequency at each point of the hologram, one can easily obtain the contribution of the corresponding elementary hologram to the complex amplitude distribution of the holographic image by multiplying its contribution to the diffraction limited amplitude with the value of the amplitude modulation transfer function (AMTF), i.e., the square root of film MTF, at the local spatial frequency. Let us denote the value of the AMTF corresponding to point ξ by $\sigma[\nu(\xi)]$. Then the complex amplitude of the reconstructed image is obtained by inserting $\sigma[\nu(\xi)]$ into the double diffraction integral Eq. (1):

$$\mathbf{V}(x,z) = \int_{\xi_1}^{\xi_2} \int_{u_1}^{u_2} \mathbf{U}(u) \frac{\cos\theta \, \cos\rho}{r_1 r_2} \sigma[(\nu(\xi)]$$

$$\times \exp[ik(r_1 - r_2)] \, du \, d\xi \ . \quad (3)$$

3.2.1 Silver halide materials (low-pass MTF)

MTF functions of common high-quality silver halide materials have been published by a number of authors (see e.g., Ref. 12, p. 94). I found that a function of the Fermi-Dirac form is a very good approximation to the AMTF of a real silver halide recording material (e.g., Agfa 8E75). The amplitude modulation transfer function takes on the following form:

$$\sigma(\nu) = \frac{1}{\exp[(\nu - \nu_0)/c] + 1} \ , \quad (4)$$

where $\nu = \nu(\xi)$ is the spatial frequency, ν_0 is the resolution limit, and c describes the slope of the curve.

The applicability of the preceding function to modeling the AMTF of silver halide holographic materials is shown in Fig. 2. The triangles are measured data taken from Ref. 12 (p. 94). The actual material is Agfa 8E75. Curve A is of the form of Eq. (4) and was fitted to the experimental data with the parameters $\nu_0 = 2800$ lines/mm and $c = 560$ lines/mm. Substituting σ from Eq. (4) into Eq. (3), we get the following formula for the complex amplitude of the holographic image recorded in a silver halide photomaterial:

$$\mathbf{V}(x,z) = \int_{\xi_1}^{\xi_2} \int_{u_1}^{u_2} \mathbf{U}(u) \frac{\cos\theta \, \cos\rho}{r_1 r_2} \frac{1}{\exp\{[\nu(\xi) - \nu_0]/c\} + 1}$$

$$\times \exp[ik(r_1 - r_2)] \, du \, d\xi \ . \quad (5)$$

3.2.2 Thermoplastic materials (bandpass MTF)

Although the holograms recorded in thermoplastic materials are surface relief gratings and hence they modify the phase of the reconstruction wave, the concept of the MTF and amplitude modulation transfer function (AMTF) is still applicable.[29] The MTF of a thermoplastic material is considerably affected by its thickness (its peak is shifted toward the higher frequencies for decreasing thickness), the development time etc.[21] The MTF of these materials is usually asymmetrical, but in certain cases even a symmetrical one such as a Gaussian function gives a good fit. A fit to a typical AMTF curve is shown in Fig. 2, curve B. Dots are experimental values after Lo et al.,[21] and the solid curve is the fit with Gaussian function. The parameters of the function are $\nu_0 = 520$ lines/mm and $w_0 = 126$ lines/mm. It can be seen that choosing this kind of model function does not introduce significant deviations from the experimental curve. On the other hand, this choice facilitates numerical calculation. Let us assume that the AMTF of the material is of the Gaussian form:

$$\sigma(\nu) = \exp\left[-\left(\frac{\nu - \nu_0}{w_0} \right)^2 \right] \ , \quad (6)$$

where ν_0 and w_0 are the center and the width of the AMTF.

Then, in the same way as for the silver halide materials, substitution of σ from Eq. (6) into Eq. (3) yields the following formula for the complex amplitude of the reconstructed image:
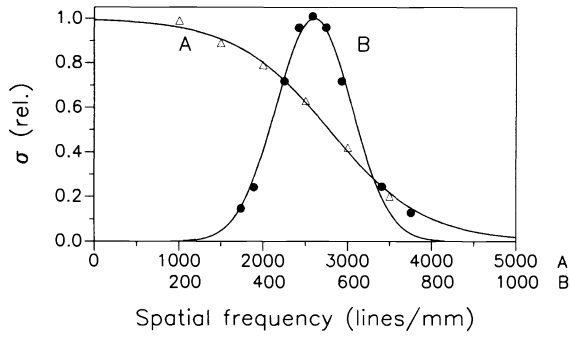
Fig. 2 Model functions of the recording materials. Solid lines represent fits with analytical functions; A: silver halide, $v_0 = 2800$ lines/mm, $c = 560$ lines/mm; B: thermoplastic, $v_0 = 520$ lines/mm, $w_0 = 126$ lines/mm. Triangles[12] and dots[21] represent measured data.
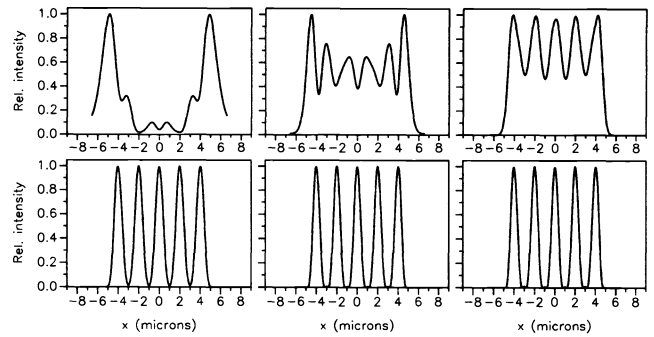

Fig. 3 Reconstructed images of the test object retrieved from holograms recorded in geometry C in silver halide recording materials of different resolving power. The resolution limits are 500, 750, 1000, 1500, 2780, and 4000 lines/mm, respectively.

$$\mathbf{V}(x,z) = \int_{\xi_1}^{\xi_2} \int_{u_1}^{u_2} \mathbf{U}(u) \frac{\cos\theta \; \cos\rho}{r_1 r_2} \exp\left[-\left(\frac{v(\xi) - v_0}{w_0} \right)^2 \right]$$

$$\times \exp[ik(r_1 - r_2)] \; du \; d\xi \; . \tag{7}$$

4 Results

Reconstructed images of test objects of different linewidths (0.5 to 4.0 μm) were evaluated for a range of values of all the main parameters of the AMTFs of the Fermi-Dirac and of the Gaussian form, as well as for a range of other recording parameters, such as the reference wave angle α_r and the separation of the on-axis object from the hologram center, R_0. To get a quantitative picture of the MTF effects, the contrast of each reconstructed image was evaluated. The contrast of the image is defined here as the integral of its intensity distribution over the transparent object lines divided by that over the opaque lines (including two opaque lines at both edges of the object).

4.1 Resolution as Function of AMTF Parameters

In one part of the following calculations, silver halide emulsions are assumed, and the parameters of their AMTFs are related by the expression $c = 560 \times v_0/2780$ (unless otherwise stated). This is not a universal rule, but a result of fitting the model function to the experimental AMTFs of several standard holographic recording materials (e.g., the Agfa materials) and gives realistic values for the slope of the AMTF.

The intensity distribution of the reconstructed image of a grating consisting of five lines of 1.0-μm width in geometry C for silver halide recording materials [with AMTFs of the form of Eq. (4)] of different resolution limit is presented in Fig. 3. The spatial frequency of the holographic grating is approximately 190 lines/mm at the lower edge, 1440 lines/mm in the center, and 2700 lines/mm at the upper edge. The quality of the reconstructed image begins to improve at $v_0 = 1000$ lines/mm, and the last two images ($v_0 = 2800$ and 4000 lines/mm) seem to be identical.

The contrast of the reconstructed image as a function of the resolution limit v_0 of the silver halide recording material has been computed for seven values of the linewidth of the grating elements: $A = 0.5, 0.7, 1.0, 1.4, 2.0, 2.8,$ and 4.0 μm
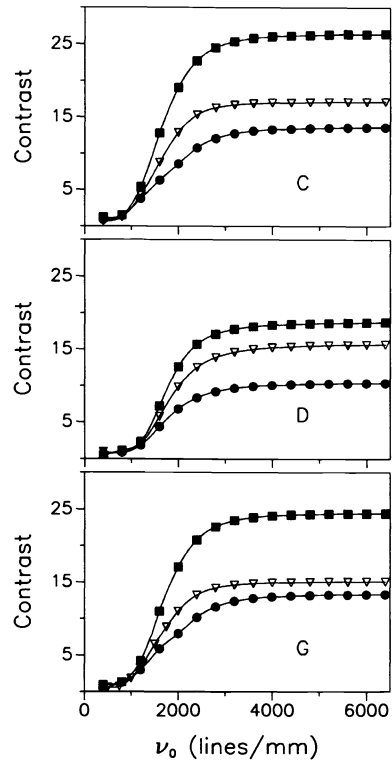
Fig. 4 Contrast of the reconstructed image versus the resolution limit of the recording material. Dots: $A = 0.7$ μm, triangles: $A = 1.0$ μm, squares: $A = 1.4$ μm. The geometries are indicated in the figure.

in geometries C, D, and G. The results for object linewidths 0.7 through 1.4 μm are shown in Fig. 4. As expected, the wider the individual lines of the grating, the higher the contrast of the reconstructed image. The diffraction limited contrast of the grating of 1.4 μm linewidth in geometry C is about twice as great as that of 0.7 μm width. For fixed linewidth and resolution limit, the contrast in geometry C is always higher than in geometry D. Because this applies even for the highest frequencies, it is a diffraction effect caused by the essential difference of the two geometries (object plane parallel or inclined to hologram plane).

Let us denote the spatial frequency at which the contrast versus resolution limit function reaches half of its diffraction
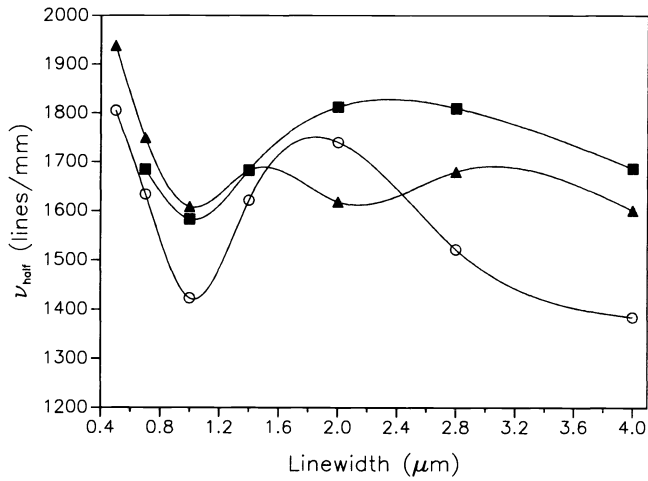
Fig. 5 Halfpoint of the contrast versus resolution limit function against the object linewidth. Circles: C geometry, squares: D geometry, triangles: G geometry.
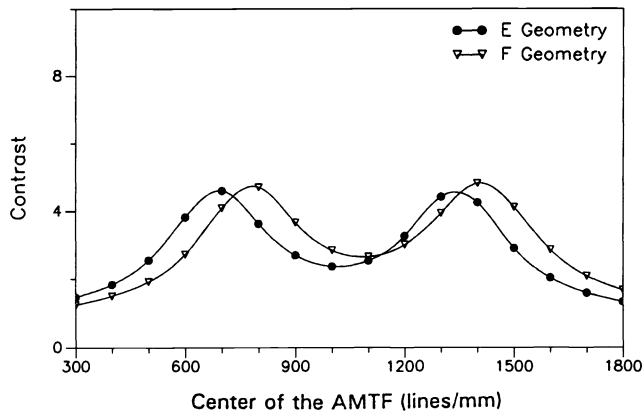

Fig. 6 Contrast of the reconstructed image versus the position of the center of the Gaussian AMTF at fixed width; $w_0 = 400$ lines/mm and $A = 1.0$ μm.

Fig. 7 Intensity distribution of the reconstructed image in geometry F, with $w_0 = 400$ lines/mm. (a) $v_0 = 800$ lines/mm, (b) $v_0 = 1100$ lines/mm, and (c) $v_0 = 1400$ lines/mm. $A = 1.0$ μm.

Fig. 8 Contrast versus parameter c at $v_0 = 1500$ lines/mm in geometry C; $A = 1.0$ μm.

limited value by v_{half}. It is a good measure of the sensitivity of the actual hologram to the resolution of the recording material. Figure 5 presents v_{half} as a function of the object linewidth in geometries C, D, and G. There are large oscillations in this function in all three recording geometries. All three curves have a definite minimum at about 1.0 μm, and the period of the oscillations increases with increasing linewidth. These oscillations are probably caused by the fact that the reconstructed image of these fine gratings is very sensitive to the position of its far-field diffraction pattern with respect to the hologram edges.

The contrast of the reconstructed image as a function of the center of the Gaussian AMTF (v_0) in geometries E and F, at a fixed value of 400 lines/mm of w_0 is shown in Fig. 6. The width of the individual object lines was 1.0 μm. Note the occurrence of two maxima in both geometries, with a peak-to-valley ratio of about 2. This fact implies that the center of the AMTF should be "fine-tuned" (e.g., by changing the thickness of the recording layer) to obtain optimal contrast in a special recording geometry. Figure 7 illustrates this comment by presenting the reconstructed images cal-
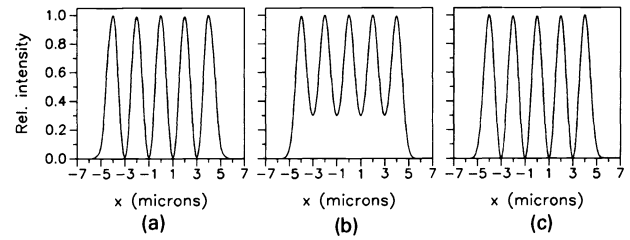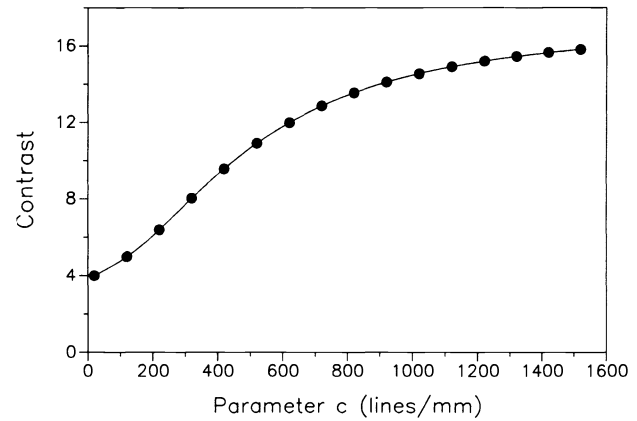
culated in geometry F with the parameters corresponding to the two peaks and the dip in Fig. 6.

A good demonstration of the superiority of the present method to the usual estimations of the MTF effects is shown in Fig. 8. The resolution limit in geometry C was fixed at $v_0 = 1500$ lines/mm, whereas parameter c (the measure of the slope of the AMTF curve) was changed from 20 to 1520 lines/mm. As c tends to 0, the AMTF curve approaches the step function. The contrast corresponding to this limit is about 4, whereas that corresponding to a realistic AMTF ($c = 320$ lines/mm) is 8, so the common methods give a considerably underestimated image resolution for a given material or an overestimated resolution limit for achieving a given contrast.

The contrast of the reconstructed image as a function of the width of the Gaussian AMTF function in geometry F is presented in Fig. 9. The parameter is v_0, the center of the AMTF. It is the curve corresponding to the lowest value of v_0 (500 lines/mm) that has the lowest values of contrast through the whole range of widths. The AMTFs centered at 800 lines/mm give better contrasts than those centered at 1000 lines/mm for widths smaller than 700 lines/mm, but the AMTFs centered at 1000 lines/mm give higher contrasts in the $w_0 > 700$ lines/mm region.

4.2 Field Range as a Function of AMTF Parameters

To determine the effects of the limited spatial resolution of the recording material on the field range, the contrast versus object position curves have been evaluated for the diffraction limited case, for two fixed values (1500 and 2800 lines/mm) of the resolution limit of a silver halide material and for one
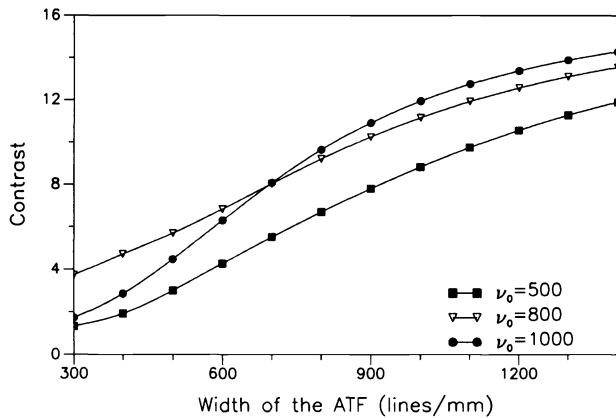
Fig. 9 Contrast of the reconstructed image versus the width of the Gaussian AMTF in F geometry; $A = 1.0$ μm.

high-resolution thermoplastic material ($\nu_0 = 1600$ lines/mm, $w_0 = 800$ lines/mm) in three geometries. The results are shown in Fig. 10. One can see at first glance that the curves corresponding to a silver halide material of $\nu_0 = 2800$ lines/mm follow very closely those corresponding to the diffraction limited image. The difference in contrast for these pairs of curves is in all cases less than 15%, because of the fact that the highest spatial frequency of the holographic gratings does not exceed considerably the resolution limit in any of the geometries. The contrast produced by the high-resolution thermoplastic is lower than that of the high-resolution silver halide but higher than that of a medium quality ($\nu_0 = 1500$ lines/mm) one.

The field range [defined as the full width at half maximum (FWHM) of the contrast versus object position curve] against the object linewidth is presented in Fig. 11. The diffraction limited field range (solid lines) is the highest in geometry G,
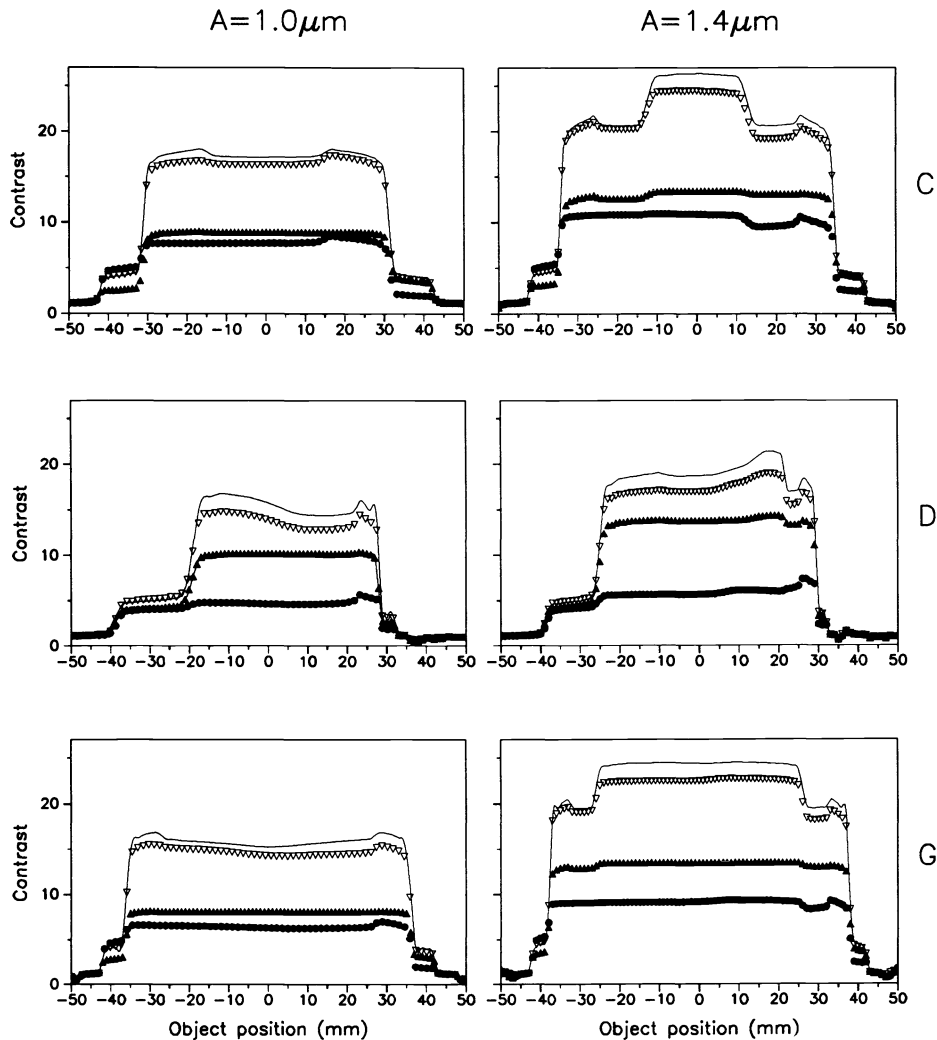

Fig. 10 Contrast versus object position. The linewidths are indicated above the columns and the geometries are indicated next to the rows. Diffraction limited images are represented by solid lines. Silver halide materials are represented by dots, $\nu_0 = 1500$ lines/mm, and open triangles, $\nu_0 = 2800$ lines/mm. Thermoplastic recording materials are represented by closed triangles, $\nu_0 = 1600$ lines/mm and $w_0 = 800$ lines/mm.
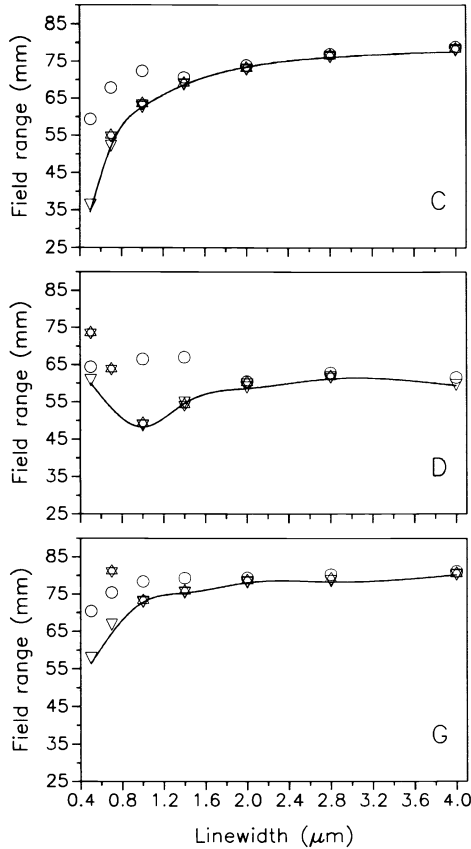
Fig. 12 Contrast versus the position of the on-axis object (R_0); $A = 1.0$ μm. Silver halide recording material.

Fig. 11 Field range versus object linewidth. Diffraction limited images are represented by solid lines. Silver halide materials are represented by circles, $\nu_0 = 1500$ lines/mm, and open triangles, $\nu_0 = 2800$ lines/mm. Thermoplastic recording materials are represented by a star of David, $\nu_0 = 1600$ lines/mm and $w_0 = 800$ lines/mm.

as expected, because it has the highest NA. One can see in both Figs. 10 and 11 that the field range in geometry D is smaller than that in geometry C, although the two geometries are of nearly the same NA (0.8). This implies that in recording geometries with a tilt between object and hologram plane, the field range is smaller than in the parallel ones. Generally, the field ranges for all the three recording materials do not differ considerably from the diffraction-limited ones except in the region below 1.4 μm where the materials of medium or poor quality practically fail to resolve the object.

4.3 Resolution as a Function of the Numeric Aperture

The contrast of the reconstructed image of the 1.0 μm ruling was evaluated for a broad range of object-to-hologram separation. All the other parameters were identical to those of geometry C. The calculations have been carried out for diffraction-limited recording and for a high-resolution ($\nu_0 = 2800$ lines/mm) and a medium-quality ($\nu_0 = 1500$ lines/mm) silver halide material. The results are shown in Fig. 12. The diffraction limited-contrast strongly oscillates in the $R_0 = 15$–120 mm region, then rapidly falls. It can be seen that recording in the high-resolution material results in nearly diffraction limited contrast, whereas that in the medium-quality one gives about half of it.
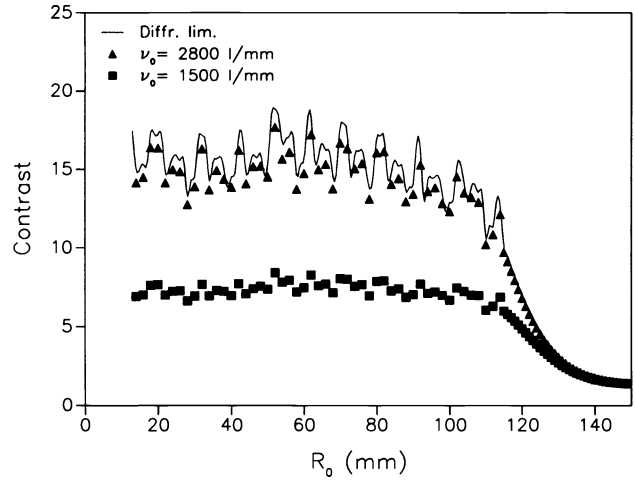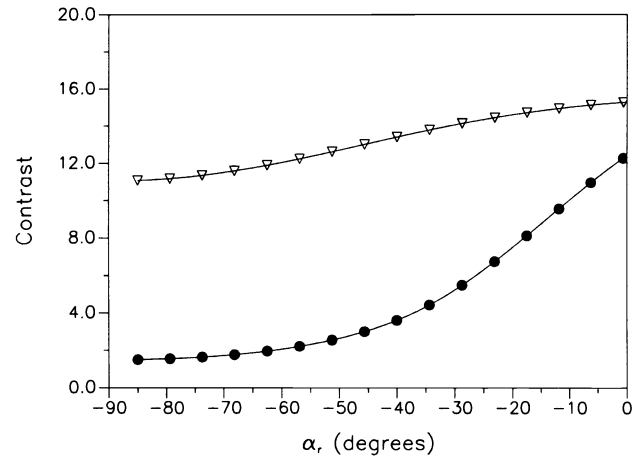

Fig. 13 Contrast versus α_r in D geometry. Silver halide recording material, dots: $\nu_0 = 1500$ lines/mm, open triangles: $\nu_0 = 2800$ lines/mm; $A = 1.0$ μm.

4.4 Resolution as a Function of the Reference Wave Angle

The proper choice of the angle of incidence of the reference wave α_r can considerably improve the quality of the holographic image. It is possible to predict the susceptibility of the image quality to changes in α_r in a given recording geometry.

The contrast of the reconstructed image against α_r at two values of ν_0 is shown in Fig. 13. The change of the contrast in the whole range of α_r is small at $\nu_0 = 2800$ lines/mm. At $\nu_0 = 1500$ lines/mm, the contrast changes by a factor of two from $\alpha_r = -40$ deg to $\alpha_r = -15$ deg.

Let us define the susceptibility of the contrast to changes in α_r as follows:

$$\Delta C = \frac{C(-5) - C(-85)}{C(-5)} , \qquad (8)$$

where $C(-5)$ is the contrast at $\alpha_r = -5$ deg and $C(-85)$ is the contrast at $\alpha_r = -85$. Figure 14 shows ΔC as a function of the object linewidth in three geometries.
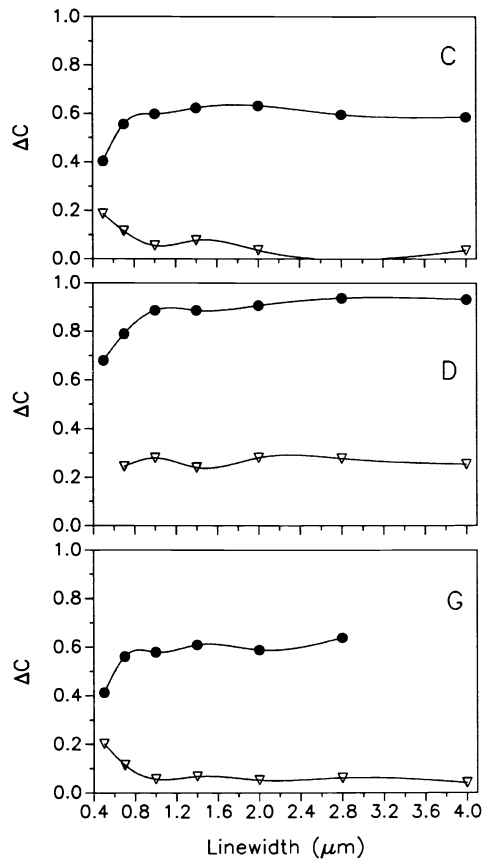
Fig. 15 Contrast of the reconstructed image versus α_r in E geometry, with $\nu_0 = 1000$ lines/mm. Upper curve: $w_0 = 1000$ lines/mm, lower curve: $w_0 = 500$ lines/mm; $A = 1.0$ μm.

Fig. 14 Susceptibility of the contrast to changes in α_r (ΔC) as a function of the object linewidth. Silver halide recording material, dots: $\nu_0 = 1500$ lines/mm, open triangles: $\nu_0 = 2800$ lines/mm.

Fig. 16 Intensity distribution of the reconstructed image in geometry E, with $\nu_0 = 1000$ lines/mm and $w_0 = 500$ lines/mm. (a) $\alpha_r = -25$ deg and (b) $\alpha_r = -10$ deg; $A = 1.0$ μm.

The thickness and other parameters of the photoconductor-thermoplastic devices can not be set easily to obtain the desired optimal amplitude modulation functions. However, the angle of incidence of the reference wave can usually be changed more or less, depending on the optical and mechanical constraints of the setup. The contrast of the reconstructed image as a function of the reference wave angle (with AMTF parameters kept constant) has been calculated in geometry E (Fig. 15). At both $w_0 = 500$ lines/mm and 1000 lines/mm, two maxima occur, however, the difference in the widths of the peaks is considerably larger at $w_0 = 1000$ lines/mm.

As a consequence of these local maxima of the contrast versus α_r curves, the reference wave angle should be carefully chosen when one wants to produce high-resolution thermoplastic holograms. This is demonstrated in Fig. 16. The left image corresponds to the peak at -25 deg of the lower curve of Fig. 15 and the right one to the -10-deg point of the same curve.

5 Conclusions

A new method was developed for the evaluation of the effects of the film MTF on the reconstructed holographic image. All the calculations presented in this paper were based on the use of the general form of the scalar Fresnel-Kirchhoff integral. The amplitude modulation transfer functions of silver halide and thermoplastic materials were modeled by analyt-
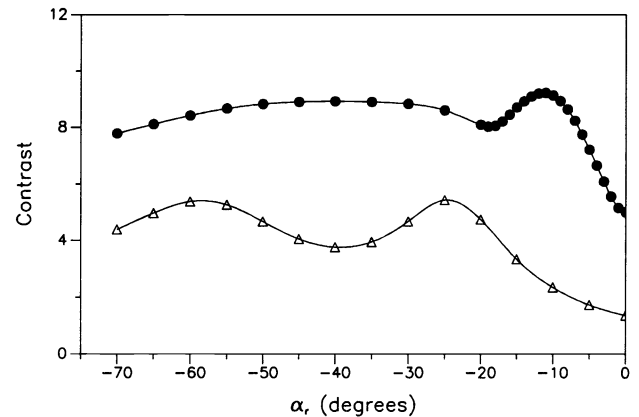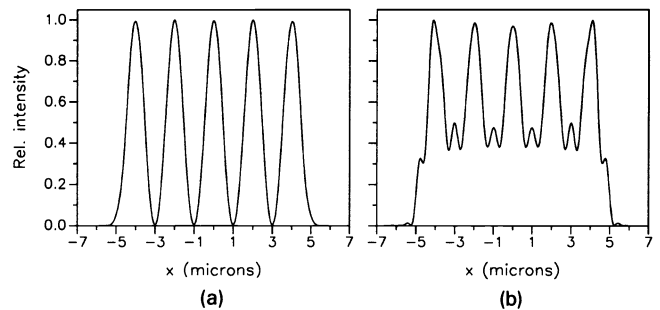
ical functions and inserted into the double diffraction integral. The capability of the method was demonstrated by means of several examples. Relationships between the contrast of the reconstructed image and the parameters of the AMTF of the recording material were established. The main results are the following.

It was found that the amplitude modulation transfer function of the recording material considerably affects the contrast of the reconstructed image, but the field range is determined mainly by the diffraction.

The importance of the slope of the AMTF curve of silver halide curves was demonstrated and the superiority of the new model function over the rectangular one was proved.

The image contrast versus the position of the center of the Gaussian AMTF function is nonmonotonic (with two peaks), whereas a monotonic dependence on the width of the AMTF has been found for the holograms studied here.

One of the predictions of the present model is that it is possible to optimize the holographic recording geometry for the actual type of recording material by a suitable choice of certain parameters. For example, in the case of certain values of the AMTF parameters of thermoplastic materials (ν_0 and w_0), there are two values of the reference angle that result in maximum image contrast.

The experimental verification of the results of the present work is in progress. Once supported by new experimental proofs, this model might become a useful tool in the design of holographic optical elements.

References

1. R. F. Van Ligten, "Influence of photographic film on wavefront reconstruction. II: cylindrical wavefronts," *J. Opt. Soc. Am.* **56**(1), 1099–1114 (1966).
2. W. Lukosz, "Equivalent-lens theory of holographic imaging," *J. Opt. Soc. Am.* **58**(8), 1084–1091 (1967).
3. J. C. Urbach and R. W. Meier, "Properties and limitations of hologram recording materials," *Appl. Opt.* **8**(11), 2269–2281 (1969).
4. T. Jannson, "Impulse response and Shannon number of holographic optical systems," *Opt. Commun.* **10**(3), 232–236 (1974).
5. A. Kozma and J. S. Zelenka, "Effect of film resolution and size in holography," *J. Opt. Soc. Am.* **60**(1), 33–44 (1970).
6. F. I. Diamond, "Magnification and resolution in wavefront reconstruction," *J. Opt. Soc. Am.* **57**(4), 503–508 (1966).
7. K. Biedermann, "A function characterizing photographic film that directly relates to brightness of holographic images," *Optik* **28**(2), 160–176 (1968/69).
8. D. G. Falconer, "Noise and distortion in photographic data storage," *IBM J. Res. Dev.* **14**(9), 521–526 (Sep. 1970).
9. A. A. Friesem, A. Kozma, and F. G. Adams, "Recording parameters of spatially modulated coherent wavefronts," *Appl. Opt.* **6**(5), 851–856 (1967).
10. R. Collier, K. Burckhardt, and L. Lin, *Optical Holography*, Chap. 10, Academic, New York, London (1971).
11. H. M. Smith, Ed., *Holographic Recording Materials*, Springer, Berlin, Heidelberg, New York (1977).
12. P. Hariharan, *Optical Holography*, Chap. 6, Cambridge University Press, Cambridge (1984).
13. W. E. Glenn, "Thermoplastic recording," *J. Appl. Phys.* **30**(12), 1870–1873 (1959).
14. J. C. Urbach and R. W. Meier, "Thermoplastic xerographic holography," *Appl. Opt.* **5**(4), 666–667 (1966).
15. R. J. Doyle and W. E. Glenn, "Lumatron: a high-resolution storage and projection device," *IEEE Trans. Electron Devices* **ED-18**(9), 739–747 (1971).
16. N. K. Sheridon, "The Ruticon family of erasable image recording devices," *IEEE Trans. Electron Devices* **ED-19**(9), 1003–1010 (1972).
17. L. H. Lin and H. L. Beauchamp, "Write-read-erase in situ optical memory using thermoplastic holograms," *Appl. Opt.* **9**(9), 2088–2092 (1970).
18. J. Gaynor, "Photosensitive deformable films," *IEEE Trans. Electron Devices* **ED-19**(4), 512–523 (1972).
19. W. C. Stewart, R. S. Mezrich, L. S. Cosentino, E. M. Nagle, F. S. Wendt, and R. D. Lohman, "An experimental read-write holographic memory," *RCA Rev.* **34**(3), 3–44 (1973).
20. W. S. Colburn and E. N. Tompkins, "Improved thermoplastic-photoconductor devices for holographic recording," *Appl. Opt.* **13**(12), 2934–2941 (1974).
21. D. S. Lo, L. H. Johnson, and R. W. Honebrink, "Spatial frequency response of thermoplastic films," *Appl. Opt.* **14**(4), 820–821 (1975).
22. P. Meyrueis, C. Liegeois, F. Lamy, and B. Ineichen, "Large aperture thermoplastic film computer holographic recording system," in *Industrial and Commercial Applications of Holography*, M. Chang, Ed., *Proc. SPIE* **353**, 40–46 (1983).
23. H. F. Budd, "Dynamical theory of thermoplastic deformation," *J. Appl. Phys.* **36**(5), 1613–1616 (1965).
24. A. I. Rabtchin, M. S. Borodkina, F. Z. Dzhabarov, Ch. A. Maksimova, V. I. Uspenskii, and V. I. Sheberstov, "On the relationship between the sensitivity of the thermoplastic plate and the threshold voltage of shearing of the polymer," *Zhurnal Nautchnoi i Prikladnoi Fotografii i Kinematografii* **12**, 149–150 (1967) (in Russian).
25. Yu. P. Gruscho and P. A. Ionkin, "Kinetics of the growth of mechanical relief in thermoplastic information recording," *Zhurnal Nautchnoi i Prikladnoi Fotografii i Kinematografii* **12**, 166–172 (1967) (in Russian).
26. H. R. Anderson, Jr., E. A. Bartkus, and J. A. Reynolds, "Molecular engineering in the development of materials for thermoplastic recording," *IBM J. Res. Dev.* **15**(3), 140–150 (1971).
27. J. C. Urbach, "Thermoplastic hologram recording," Chap. 6 in *Holographic Recording Materials*, H. M. Smith, Ed., pp. 161–207, Springer-Verlag, Berlin, Heidelberg, New York (1977).
28. I. Bányász, G. Kiss, and P. Varga, "Holographic image of a point source in presence of misalignment," *Appl. Opt.* **27**(7), 1293–1297 (1988).
29. I. Bányász, "Resolution problems in holography," in *International Colloquium on Diffractive Optical Elements*, J. Nowak and M. Zajac, Eds., *Proc. SPIE* **1574**, 282–293 (1991).
30. H. M. Smith, *Principles of Holography*, p. 122, John Wiley & Sons, New York (1975).
31. J. Nowak and M. Zajac, "Numerical investigations of holographic imaging quality," *Opt. Appl.* **15**(3), 239–248 (1985).
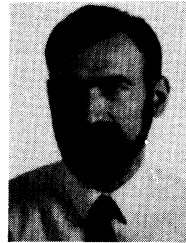
István Bányász received his diploma in physics in 1983 and PhD in physics in 1987 from Eötvös Loránd University, Budapest, Hungary. His main research field is the theory and practice of high-resolution holography. He has also carried out research in holographic interferometry and holographic recording materials. Dr. Bányász received the prize of the Hungarian Academy of Sciences for young scientists in 1993. Currently he is working toward the refinement and experimental verification of a model of holography. He is the author of 19 papers.